scientific reports

Check for updates

OPEN

Ultralow-dose irradiation enables engraftment and intravital tracking of disease initiating niches in clonal hematopoiesis

Kevin Lee[1,2,13], Wimeth Dissanayake[2,3,13], Melissa MacLiesh[2,3], Cih-Li Hong[2,4], Zi Yin[5], Yuko Kawano[6,12], Christina M. Kaszuba[1,6], Hiroki Kawano[6,12], Emily R. Quarato[6,7], Brian Marples[8], Michael Becker[9], Jeevisha Bajaj[6,10], Laura M. Calvi[2,6,11,12] & Shu-Chi A. Yeh[1,2,4,6]✉

Recent advances in imaging suggested that spatial organization of hematopoietic cells in their bone marrow microenvironment (niche) regulates cell expansion, governing progression, and leukemic transformation of hematological clonal disorders. However, our ability to interrogate the niche in pre-malignant conditions has been limited, as standard murine models of these diseases rely largely on transplantation of the mutant clones into conditioned mice where the marrow microenvironment is compromised. Here, we leveraged live-animal microscopy and ultralow dose whole body or focal irradiation to capture single cells and early expansion of benign/pre-malignant clones in the functionally preserved microenvironment. 0.5 Gy whole body irradiation (WBI) allowed steady engraftment of cells beyond 30 weeks compared to non-conditioned controls. In-vivo tracking and functional analyses of the microenvironment showed no change in vessel integrity, cell viability, and HSC-supportive functions of the stromal cells, suggesting minimal inflammation after the radiation insult. The approach enabled in vivo imaging of *Tet2*$^{+/-}$ and its healthy counterpart, showing preferential localization within a shared microenvironment while forming discrete micro-niches. Notably, stationary association with the niche only occurred in a subset of cells and would not be identified without live imaging. This strategy may be broadly applied to study clonal disorders in a spatial context.

Keywords Clonal hematopoiesis, Myelodysplastic syndrome, Fluorescence imaging, Time-lapse imaging, Multiphoton microscopy, Cancer microenvironment, TET2

Clonal hematopoiesis of indeterminate potential (CHIP) is originated from clonal expansion of hematopoietic stem cells (HSCs) and their progenies that carry mutations associated with hematological cancer (*e.g., DNMT3a, TET2, ASXL1*). It is associated with increased risks of myeloid malignancies, cardiovascular diseases and all-cause mortalities[1,2] that positively correlate with the mutant clone size. For this reason, elucidating the mechanisms regulating mutant clonal expansion while preserving healthy hematopoiesis has been under intensive investigations[3–10] to better understand pathogenesis and intervention.

[1]Department of Biomedical Engineering, University of Rochester, Rochester, NY, USA. [2]Department of Orthopaedics, Center for Musculoskeletal Research, University of Rochester Medical Center, Rochester, NY 14623, USA. [3]Department of Biology, University of Rochester, Rochester, NY, USA. [4]Department of Physiology/Pharmacology, University of Rochester Medical Center, Rochester, NY, USA. [5]Institute of Optics, University of Rochester, Rochester, NY, USA. [6]Wilmot Cancer Institute, University of Rochester Medical Center, Rochester, NY, USA. [7]Department of Toxicology, University of Rochester Medical Center, Rochester, NY, USA. [8]Department of Radiation Oncology, University of Rochester Medical Center, Rochester, NY, USA. [9]Department of Medicine, Indiana University, Indianapolis, IN, USA. [10]Department of Biomedical Genetics, University of Rochester Medical Center, Rochester, NY, USA. [11]Department of Pathology and Laboratory Medicine, University of Rochester Medical Center, Rochester, NY, USA. [12]Department of Medicine, University of Rochester Medical Center, Rochester, NY, USA. [13]These authors contributed equally: Kevin Lee and Wimeth Dissanayake. ✉email: ShuChi_Yeh@URMC.Rochester.edu

Notably, though the leukemogenic mutations underlying CHIP could occur early in life, CHIP primarily manifests in the elderly, indicating that coordinated cell-autonomous and extrinsic factors modulate dominance of the healthy or mutant clones. To this point, it has been consistently reported that systemic low-grade inflammation of the marrow microenvironment confers competitive advantages of the mutant cells[4,5,7–10]. In addition to systemic factors, advances in imaging technology revealed that spatial organization of healthy and malignant hematopoietic cells in the bone marrow regulates cell expansion capability and lineage commitment[11–20]. For example, we previously showed that expansion of HSCs and Meis1/HoxA9 -driven AML cells can only be supported by restricted bone marrow cavities with bone resorption activities, but not cavities predominated by bone deposition[17,20]. Notably, recent work in myeloproliferative neoplasms revealed differential cell expansion and disease phenotypes when the mutant clones carrying the same driver mutation are associated with distinct niches[19]. These results strongly suggested that spatial organization of the cells governs functional heterogeneity and disease progression, yet this has not been elucidated in CHIP.

We reason that our ability to pinpoint and decode the niche in pre-malignant clonal disorders, including CHIP, is largely limited by the lack of a working model to visualize the disease initiating cells in a functional microenvironment. Of note, at the early disease stage, the niche is a spatially restricted micro-anatomical location surrounding rare mutant clones. The niche will only represent a small fraction of total bone marrow cells given the low frequency of Lin^-/c-Kit^+/$Sca1^+$cells (LSK ~ 0.16%)[21] and a low percentage of the mutant cells in CHIP. This subset would be much smaller at the emergence of mutant clones and would not be easily captured via bulk cell isolation where spatial context is lost. An ideal approach is to generate a chimera that carries color-distinct healthy HSCs mixed with a very small fraction of mutant cells. This depends on the availability of conditional multi-genetic models[9], by combining Dox- and CreER/loxP systems under the control of HSC-specific promoters. In vivo tracking of these models will likely still be limited by accessibility, as the cells induced for mutation may not always appear in the intravital imaging window (mostly through calvarial bone marrow[22] as the least invasive approach). For these reasons, transplantation of congenic reporter cells has been a standard approach to model CHIP and other bone marrow failure disorders[19,23,24], but this approach requires genotoxic conditioning for the non-malignant cells to engraft, which compromises host hematopoiesis and the microenvironment[25]. Specifically, both vascular integrity and MSCs are frontline responders to radiation-induced inflammation[26] and have been shown to be critical in regulating HSC maintenance, directly and/or indirectly through modulating microenvironment (e.g., propensity of osteo- vs. adipogenesis and immune responses)[27–35]. Alternatively, injecting a high number of cells (1.5×10^7 cells) enabled successful engraftment in non-conditioned mice[23,24]. However, challenges remain when attempting to model early clonal expansion events from solitary cells, as this high cell dose led to crowds of cells seeding into the same marrow space. Cell-derived factors from a crowd of seeded cells likely start to remodel the microenvironment, compromising endosteal and vascular niches[36].

In this work, we leveraged high-resolution live-animal microscopy and ultralow dose (0.5 Gy) whole body or focal irradiation on unilateral side of calvaria to enable engraftment and sensitive detection of single cells in a functionally preserved microenvironment. The approach thus enabled the first in vivo imaging of *Tet2*$^{+/-}$ and the healthy counterpart, showing preferential localization within a shared microenvironment with healthy and mutant cells forming discrete micro-niches. Stationary association with the niche only occurred in a subset of cells and would not be identified without live imaging. The developed strategy utilizes the lowest irradiation dose to allow engraftment reported in the field to date, demonstrates minimal impact on the microenvironment, and may be broadly applied to study other bone marrow failure disorders in spatial context.

Results

0.5 Gy irradiation allows in vivo tracking of non-malignant cells

To examine the feasibility of studying clonal competition, it is necessary to create a model that allows stable engraftment of benign clones in the minimally perturbed microenvironment. We transplanted healthy donor cells from UBI-GFP adult mice (2×10^6 whole bone marrow) into non-irradiated vs. 0.5 Gy WBI recipients. As demonstrated via intravital imaging of the mouse calvaria and peripheral analyses of the recipient animals (Fig. 1a), 0.5 Gy irradiation enabled direct visualization of rare single cells and cells that underwent early expansion in vivo at 1 week after transplantation. Cells continued to expand in the bone marrow beyond early time points, and the engraftment in the marrow continued to be observed at 10 months after transplantation (Fig. 1b,e, Fig. S1a, Movie S1). To further minimize the radiation insult, we used the small-animal radiation research platform (SARRP) to allow uniform targeting of 0.5 Gy irradiation on the unilateral (right) side of calvaria (Fig. 1c). Notably, local irradiation regimen enabled cell survival and early expansion in both irradiated and non-irradiated sides (Fig. 1d). Flow cytometry analyses revealed steady engraftment of cells through 30 weeks in the 0.5 Gy whole body irradiated mice compared to non-conditioned controls, where engraftment was negligible (Fig. 1b,e). An increase in the irradiation dose to 1 Gy was found to boost the engraftment (Fig. S1b), however we opted for the lower dose in the interest of preserving the bone marrow microenvironment as much as possible. In comparison to WBI, local irradiation on the right side of the calvarial bone still provided borderline engraftment but showing an overall lower fraction of donor cells detected in the peripheral blood (Fig. 1f). Such uncertainty makes this approach less robust for long-term in vivo tracking as the fraction of donor cells reduced beyond 16 weeks, while with a potential merit for allowing short-term tracking up to 12 weeks.

Vascular integrity in the bone marrow was maintained after 0.5 Gy WBI

Inflammation and increased vascular permeability are known to compromise HSC maintenance[37]. In addition, vessel dilation and permeability are sensitive indicators of inflammatory responses associated with radiation[25,26,38]. Therefore, we reason that measuring changes in vascular integrity provides a fair assessment of the bone marrow microenvironment after 0.5 Gy WBI. At 1 week after irradiation, via intravenous administration of a vascular

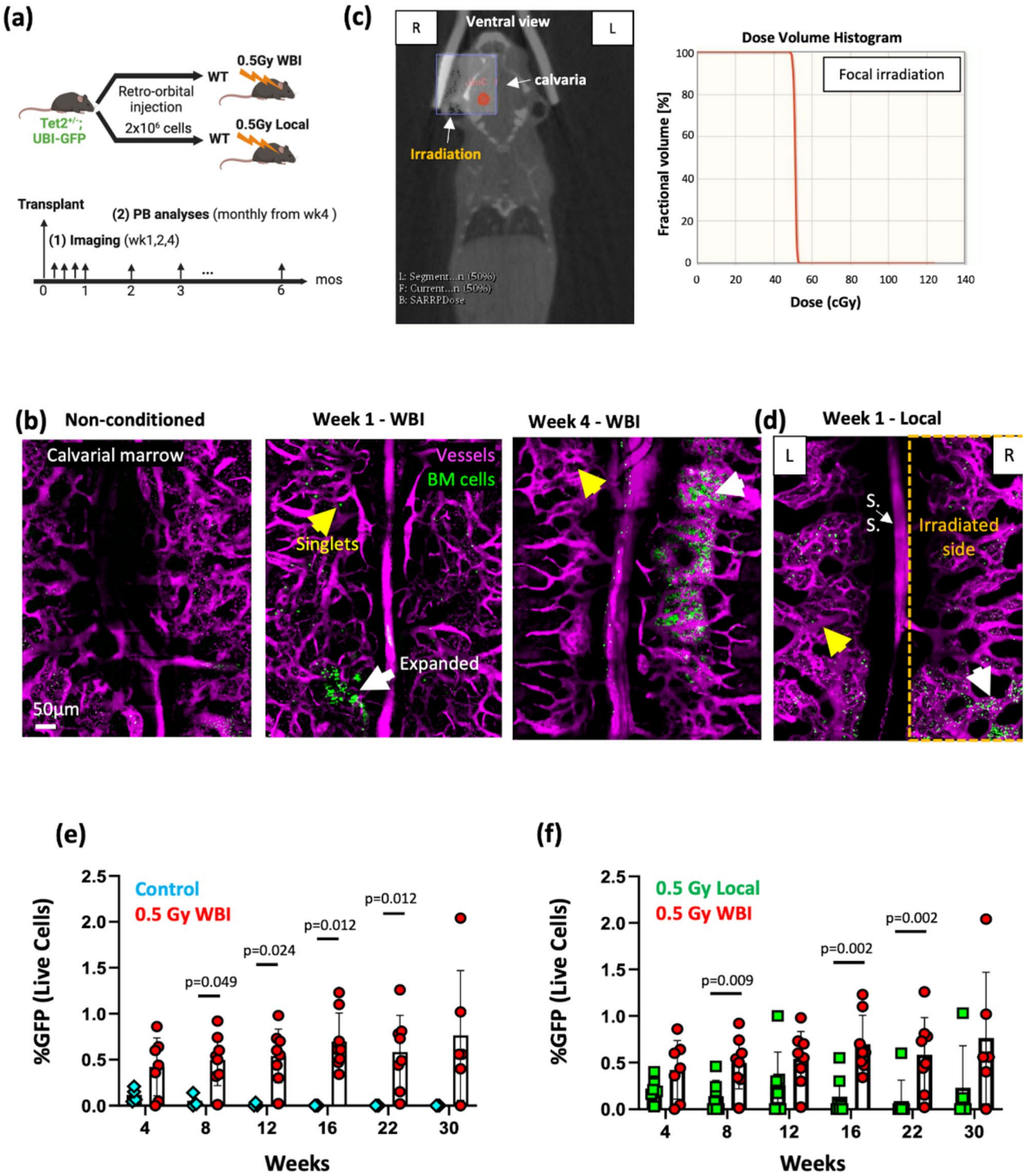

Fig. 1. Low-dose (0.5 Gy) irradiation enables engraftment and tracking of healthy hematopoietic cells in vivo. (**a**) Timelines of the transplantation, imaging and peripheral blood analyses. (**b**) Maximum intensity projection of a montage of tile-scanned z-stacks showed single cells (yellow arrows) and cells that underwent expansion (white arrows) at 1 and 4 weeks after transplantation into 0.5 Gy whole body irradiated recipient mice, compared to the non-conditioned control (Green, UBI-GFP cells; Magenta, Rhodamine dextran; representative images from N = 3—7 mice). (**c**) Strategies of small-animal radiation research platform (SARRP) local irradiation. Ventral view of the animal and placement of calvarial-targeted isocenter (red) and radiation field (10 × 10 mm, purple square). The dose volume histogram shows 100% of 0.5 Gy dose targeted to only the radiation field. (**d**) Maximum intensity projection of a montage of tile-scanned z-stacks showed cell engraftment in the non-irradiated site, at 1 week after transplantation into 0.5 Gy local irradiated recipient mice (Green, UBI-GFP cells; Magenta, Rhodamine dextran; representative images from N = 3 mice). (**e**,**f**) Engraftment analyses (GFP^+ cells in the peripheral blood) after transplantation of 2×10^6 GFP^+ whole bone marrow cells in 0.5 Gy whole body irradiated (WBI), non-conditioned, and 0.5 Gy locally irradiated recipients (N = 3–8 mice per experimental group). Each dot represents an individual mouse. Data from all mice are shown. Two-sided Mann–Whitney test. Data shows mean ± s.d.

contrast dye conjugated to high molecular weight molecules (Rhodamine dextran (70 kDa)), simultaneously with video-rate tracking (15–30 frames/second) of the dye perfused into the interstitial space (Movie S2), we showed that the vascular barrier was preserved, without signs of diffusive dye leakage. The hot spots of high permeability remained mainly near peri-sinusoidal zones (vessel diameter > *15* μm) as reported previously[37] (Fig. 2a,b). In contrast, mice that received 4.5 Gy WBI exhibited significantly increased vascular permeability even though vessel dilation was not noted. Vessel dilation and density changes were not observed when measured at one week after irradiation between control and 0.5 Gy WBI group (Fig. 2c,d), as also demonstrated in locally irradiated cases (Fig. 1d). Although the preserved vascular integrity suggested minimal inflammation elicited by 0.5 Gy irradiation; transcriptionally, immune cells exhibited an upregulated inflammatory response at 1 week after 0.5 Gy irradiation (Fig. S2b). The downregulated ribosome pathways, however, may suggest an impaired rRNA and protein synthesis in response to the stress and may explain the increase in donor cell engraftment compared to non-conditioned control[39].

In vivo live/dead imaging and fluorescent activated cell sorting (FACS) analyses showed preserved cell viability after 0.5 Gy irradiation

Irradiation induces cell death that could occur within a day or after a few cell divisions[40]. To evaluate cell death of the overall hematopoietic and non-hematopoietic populations in the bone marrow, propidium iodide (PI) was delivered intravenously to label dead cells 1 day after the animal received 0.5 Gy WBI. PI-labeled cells in each bone marrow cavity were than enumerated. Note that the marrow "cavity" refers to the concave 3D inclusions in the endosteal zone[17] and its margin was defined based on segmentation of the bone structure. As shown in Fig. 2e,f, at 1 day after irradiation, the number of PI^+ cells per unit volume in each cavity was not altered significantly in the 0.5 Gy irradiated group compared to the age-matched control group, whereas a substantial increase of cell death was observed in the 4.5 Gy irradiated group. Additionally, FACS analyses of bone marrow endothelial ($Cd45^-$, $Ter119^-$, $Cd31^+$)[41] and stromal ($CD51^+$, $Sca1^+$, $Cd45^-$, $Ter119^-$, $Ly6C^-$, $Cd31^-$)[42] niche populations showed that cells remained highly viable at 1 week after 0.5 Gy irradiation (Fig. 2g,h).

Tri-lineage differentiation of MSCs and the hematopoietic support are maintained after 0.5 Gy irradiation

MSCs are major constituents in the peri-vascular niche known to support hematopoiesis, and their lineage differentiation propensity has been shown to regulate leukemia progression[27–35]. To characterize functional alterations induced by low-dose irradiation, MSCs were harvested from mice at 1 week after 0.5 Gy WBI and from the age-matched non-irradiated mice, followed by assays to examine their tri-lineage differentiation and hematopoietic support capacity. As shown in Fig. 3a,b, 0.5 Gy WBI did not result in a significant reduction of the tri-lineage differentiation capacity or induce differentiation bias. The fractional area stained with Alizarin Red (osteogenesis), Oil Red (adipogenesis), or Alcian Blue (chondrogenesis) were unchanged between groups.

Quantifying the key hematopoietic niche factor, CXCL12, in bone marrow interstitial fluid at 1 week after irradiation, we showed that CXCL12 secretion remained unchanged in 0.5 Gy irradiated group, but significantly reduced in mice receiving 4.5 Gy irradiation (Fig. 3c). Furthermore, to determine whether 0.5 Gy WBI may reduce the capacity of MSCs in supporting hematopoiesis, we co-cultured MSCs with Lin^-/ $Sca1^+$/ $c\text{-}kit^+$ (LSK) cells harvested from UBI-GFP donors for 72 h, followed by transplantation of the GFP^+ LSK cells into lethally irradiated recipients. Peripheral blood analyses of GFP cells showed comparable chimerism between the irradiated and control groups through week 4 to week 16 (Fig. 3d), supporting that the key secreting factors to support HSCs are preserved at the one-week time point after irradiation.

Intravital imaging revealed a high frequency of *Tet2*$^{+/-}$ and WT (*Tet2*$^{+/+}$) cells cohabitating the same bone marrow cavity while a subset forming discrete micro-niches

Taking advantage of the 0.5 Gy WBI protocol and intravital imaging, we were able to track the co-transplanted *Tet2*$^{+/-}$ and WT (*Tet2*$^{+/+}$) clones in a functionally preserved microenvironment. Strikingly, the results demonstrated a high frequency of the two populations cohabitating the same bone marrow cavity, as shown in the x–z cross-sectional view (Fig. 4a). Out of surveyed marrow cavities where the transplanted cells were identified, a majority of these cavities were found to house both WT and the *Tet2*$^{+/-}$ clones, observed both in calvaria and long bone metaphysis (Fig. 4b, Fig. S3). Interestingly, *Tet2*$^{+/-}$ cells did not necessarily exhibit competitive advantages (Fig. 4c). The results implied the presence of hot spots (shared marrow cavities) where two clones compete. It was also noted that, despite residing in the same marrow cavity, the WT and *Tet2*$^{+/-}$ cells mostly segregate with their own clones. In contrast, WT and *Tet2*$^{+/-}$ cells exhibited a mean Euclidean distance of 155 μm away from each other (Fig. 4d). The results suggest that the two clones likely relied on distinct micro-niches at the initiation stage of clonal development. Via longitudinal tracking of cell displacement, we further showed that only a subset of clusters had stable association with the microenvironment where cells essentially stayed stationary over an hour of the observation period (Fig. 4e,f, orange box, Movie S3). In contrast, a stable "niche" may not be present for a substantial fraction of the highly motile *Tet2*$^{+/-}$ population, implying less reliance on the microenvironmental signals in this subset (37%, Fig. 4e,f, blue box). The ability to resolve spatial landscape of CHIP development in a functional microenvironment thus paves ways for downstream analyses to identify the niche-associated subsets and to understand microenvironment factors involved in the clonal competition processes.

Discussions

Our work here describes the use of 0.5 Gy WBI and intravital imaging to enable the first in vivo tracking of non-malignant hematopoietic cells in minimally perturbed, functional microenvironment. To our knowledge, 0.5 Gy is the lowest reported dose that has been used to study clonal hematopoiesis. We characterized the engraftment

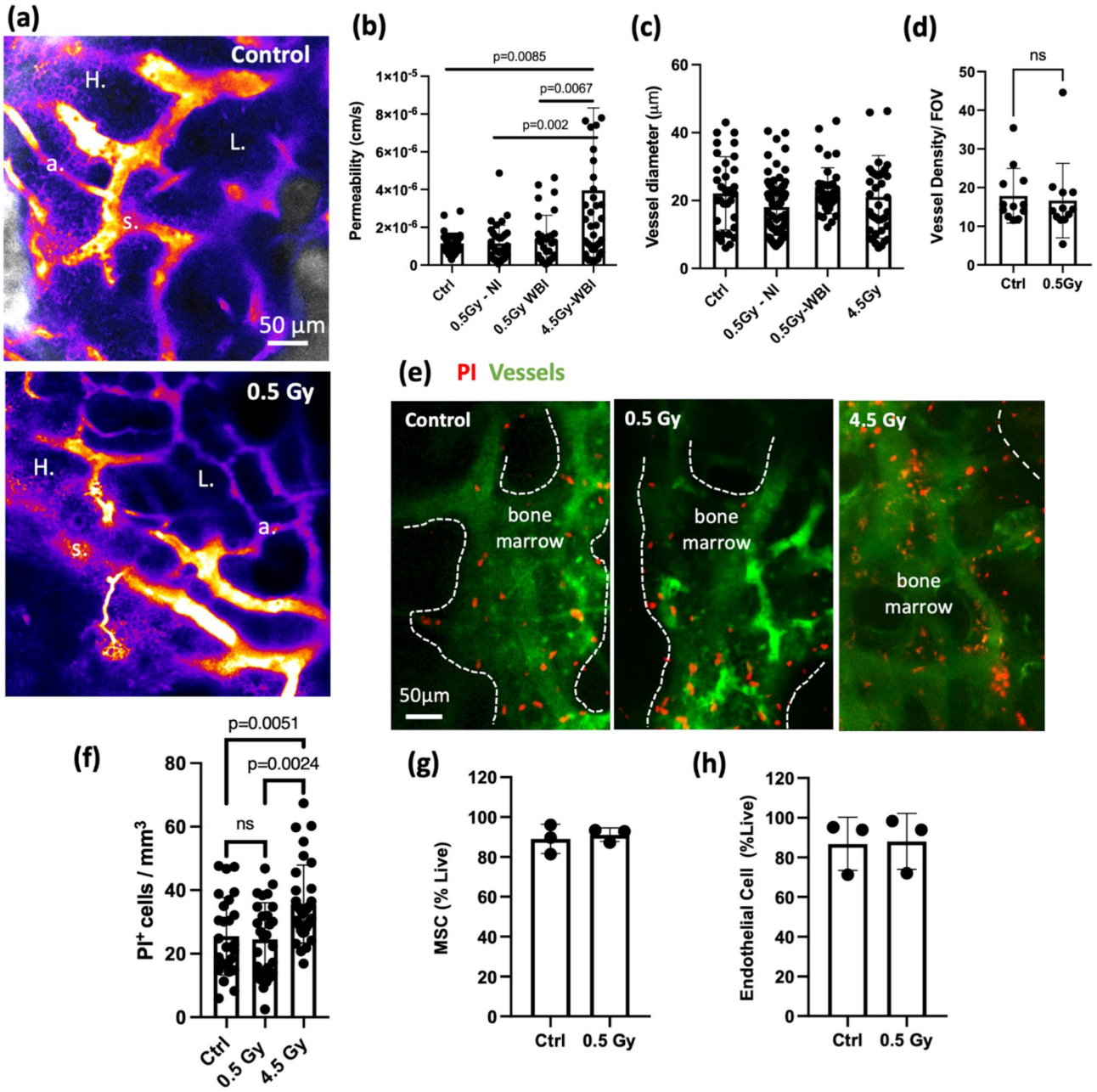

Fig. 2. Vascular integrity and cell viability are preserved after 0.5 Gy whole body irradiation. (**a**) Heat maps showing average intensity projection from the first 8 seconds of rhodamine—dextran leakage after the dye was administered retro-orbitally. Bright color indicates higher pixel intensity (s: sinusoidal vessels with diameter > 15 µm; a: arterioles with diameter < 12 µm; H: high permeability zone; L: low permeability zone). (**b**,**c**) Average vascular permeability and diameter measured in whole body irradiated (WBI), non-irradiated (Ctrl), and locally irradiated mice. (Each data point represents measurements from individual vessel segments. n = 33–73 segments. N = 3 mice from 0.5 or 4.5 Gy WBI and Local groups, N = 2 mice from Ctrl). (**d**) Vascular density characterized in fraction of dextran$^+$ voxels field of view between 0.5 Gy WBI and non-irradiated (Ctrl) groups 1 week after 0.5 Gy irradiation, Two-sided Mann–Whitney test. Data shows mean ± s.d. (**e**) Maximum intensity projection of representative z-stacks of bone marrow cavities. Images were taken from day 1 after 0.5 Gy, 4.5 Gy WBI or from a non-conditioned mouse (Red: propidium iodide; Green: Fluorescein-dextran). (**f**) Quantifications of PI$^+$ cells per unit volume from the measured cavities (n = 6–9 cavities, N = 3 mice). Osteocytes (determined by the lacuna space from the bone channel) are excluded throughout the analyses as all osteocytes are labeled with propidium iodide in both groups. Two-sided Mann–Whitney test. Data shows mean ± s.d. (**g**,**h**) FACs analysis of endothelial and stromal cell populations 1 week after 0.5 Gy WBI (n = 3 vials cell suspension pooled from N = 5 mice, two-sided unpaired t-test).

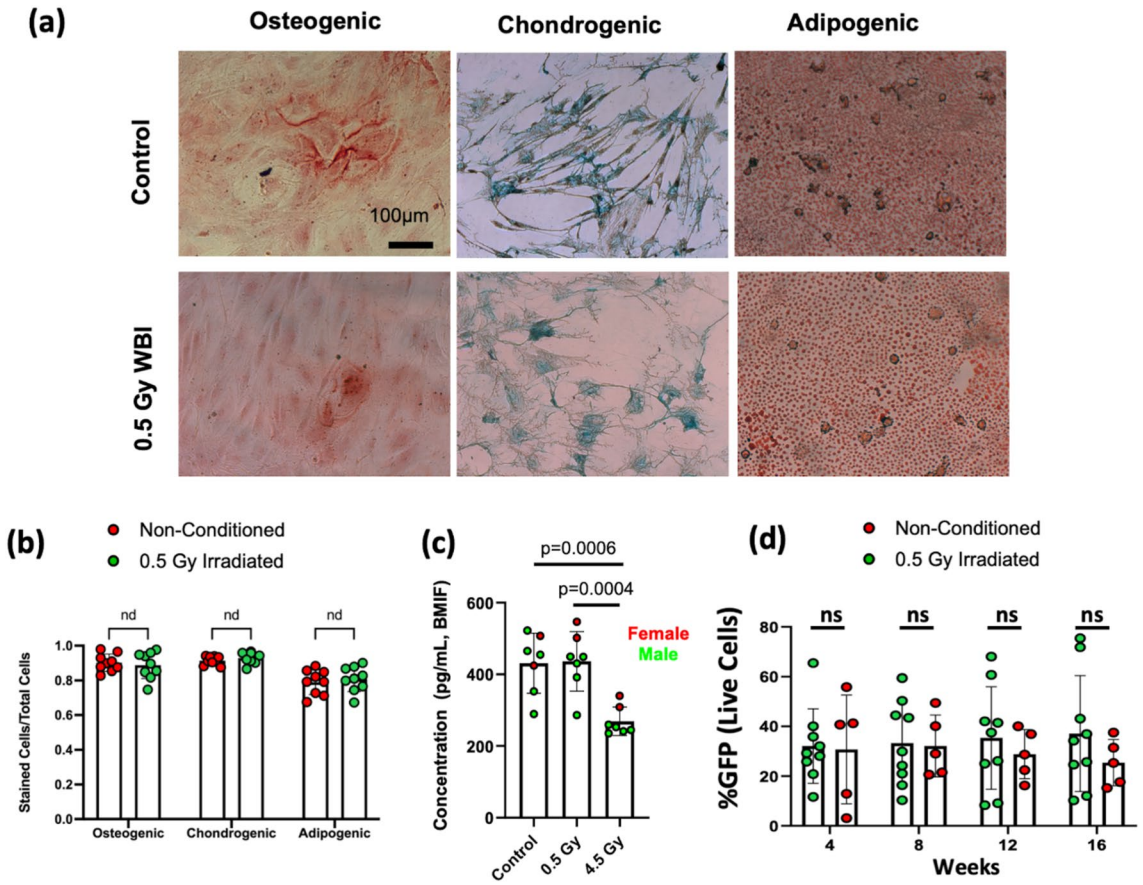

Fig. 3. Tri-lineage differentiation of MSCs and the hematopoietic support are maintained after 0.5 Gy irradiation. (**a**) Representative images from osteogenic (Alizarin Red staining), adipogenic (Oil Red staining) and chondrogenic (Alcian Blue staining) assays. (**b**) Quantifications of tri-lineage differentiation capacity based on the number of labeled cells out of total cells. (Each data point represents measurements from replicates. n = 3 replicates per mouse. N = 3 mice per group). (**c**) CXCL12 ELISA performed on total bone marrow interstitial fluid taken from non-conditioned mice, 0.5 Gy WBI mice and 4.5 Gy WBI mouse (n = 2 replicates per mouse, N = 7 mice per group, Two-sided unpaired t-test). (**d**) Engraftment analyses (GFP^+ cells in the peripheral blood) of LSK cells transplanted to lethally irradiated mice. LSK cells were co-cultured with MSCs undergoing 0.5 Gy WBI (green) vs the control group (red). Each dot represents a replicate. (n = 2–3 replicates per mouse. N = 3 mice per group, Two-sided Mann–Whitney test. Data shows mean ± s.d.).

and hematopoietic microenvironment in such setting and showed that 0.5 Gy WBI allows long-term engraftment compared to non-conditioned host animals. The preserved vascular architecture, cell viability, tri-lineage differentiation, and hematopoietic support of MSCs indicated minimal adverse impacts, such as inflammation, imposed by this irradiation regimen. The imaging protocol revealed the presence of hot spots where clonal competition take place that warrants spatially resolved analyses under image-guidance.

One notable advantage of using intravital imaging is the ability to identify single cells and early cell expansion within highly localized marrow microdomains. These rare cell population at the clonal initiating stage and the spatial information of their niche are otherwise not attainable through peripheral blood or whole bone marrow analyses where cells were harvested in bulk. The work thus provides a novel working model to study the marrow microenvironment of pre-malignant clonal disorders, taking spatial context into consideration. Importantly, in vivo imaging can visualize sites of clonal competition between pre-malignant cells that carried leukemia-associated mutations and the healthy counterpart, and the approach may be broadly applied to study other bone marrow failure disorders that manifest aplasia vs. abnormal expansion, such as myeloproliferative neoplasms.

Of note, irradiation is known to induce inflammation and compromise vascular integrity[26]. In general, an irradiation threshold of 2 Gy has been reported to induce secretion of pro-inflammatory mediators, degradation of endothelial junction and an increase in vascular permeability[43]. In agreement with these findings, we did not observe compromised vascular barrier (an increase in permeability) at the irradiation dose of 0.5 Gy. Note that erythro-lineage cells are highly sensitive to irradiation, which can result in hemolysis and iron overload in the bone marrow. Consequently, excessive iron also reduces VE-cadherin and deteriorates endothelial barrier. Apoptosis of erythroblasts were found at an irradiation dose of > 4 Gy[44]. Our results that showed intact vascular integrity after 0.5 Gy irradiation thus implied minimal inflammation and iron overload in the hematopoietic microenvironment.

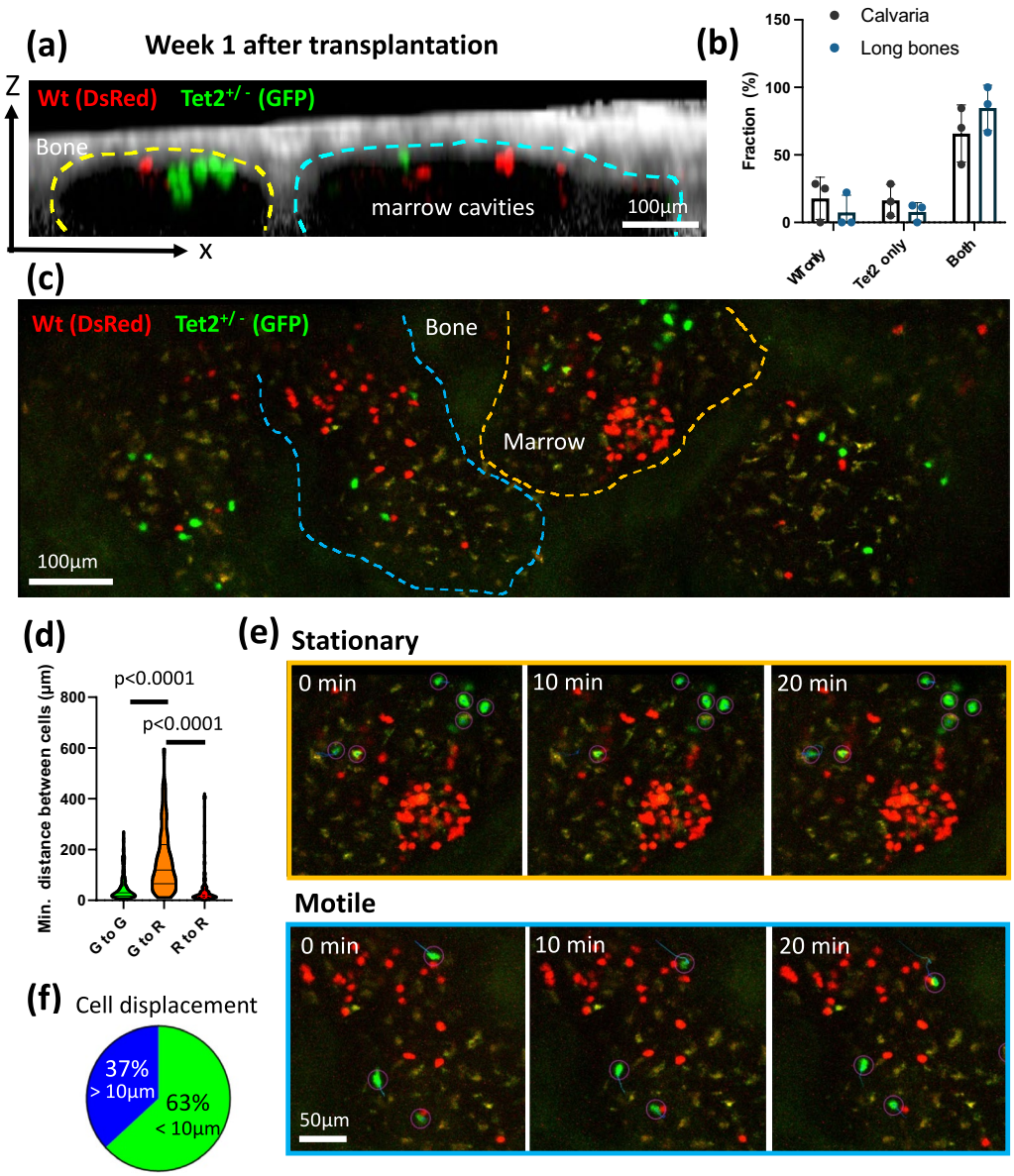

Fig. 4. Intravital imaging revealed a high frequency of Tet2$^{+/-}$ and WT (Tet2$^{+/+}$) cells cohabitating the same bone marrow cavity while a cell subset formed discrete micro-niches. (**a**) A sagittal section of bone marrow cavities (yellow and cyan dashed lines) containing transplanted WT (red) and Tet2$^{+/-}$ (green) cells. (**b**) The frequency of a single population (Tet2$^{+/-}$ or WT alone) or both populations found in the same bone marrow cavity. Data are analyzed from cavities where cells were present, from calvaria and freshly isolated tibia metaphysis. (n = 47 cavities from calvaria, 23 cavities from long bones, N = 3 mice per group) (**c**) Representative maximum intensity projected images showing growth advantages from the WT or the Tet2$^{+/-}$ clones at 1–2 weeks after transplantation. (**d**) The minimal inter-cellular distance between the same clone (Green-to-Green distance or Red-to-Red distance) or between Tet2$^{+/-}$ and the WT clones (Green-to-Red distance) in the same bone marrow cavity. Each data points were measured based on 3D coordinates between a cell and its closest cell (n = 180, 180, 205 data points for G–G, G–R, R–R, respectively. N = 3 mice, Two-sided Mann–Whitney test. Data shows full range, median, the first and third quartiles.) (**e**) Time-lapse acquisition showing stationary vs. motile cell population with their trajectories. Images were displayed in 2D by maximum intensity projection. (**f**) The fraction of stationary vs. motile cell population. Quantifications was based on Tet2$^{+/-}$ cell displacement greater than 10 μm in 3D over an 1 h with 1-min time interval (n = 19 cells, N = 4 mice).

The study also focused on functional assessment of MSCs as the MSCs constitute a key HSC niche. In the context of myeloid disorders, the population mediates proinflammatory cytokines in myelodysplastic syndromes and chemoresistance in leukemia[27–35,37]. In addition, the tri-lineage differentiation capacity of MSCs impacts

hematopoiesis in several ways. Lineage bias of HSCs and hematopoietic recovery are regulated differentially by factors released by osteo-primed or adipo-primed MSC populations[14,45,46]. Under 0.5 Gy irradiation, our results revealed preserved tri-lineage differentiation capacity of MSCs. Moreover, healthy LSK cells co-cultured with irradiated stromal cells demonstrated a reconstitution capacity comparable to the LSK cells co-cultured with the non-irradiated control group. Additionally, CXCL12 levels in the bone marrow interstitial space remains unchanged under 0.5 Gy irradiation but is significantly decreased under 4.5 Gy irradiation. The results are consistent with prior findings that showed negligible adverse effects from 0.1 to 1 Gy[47] on human MSCs and negligible changes in osteogenic potential. However, irradiation doses beyond 2 Gy significantly reduced MSC colony formation and survival[48]. It is worth noting that, although key hematopoietic support factors such as CXCL12, IL-3, were recovered when examined at 4 weeks after 4–8 Gy irradiation[31], at the common sublethal dose (6 Gy), it was found to induce a sustained decrease of host short-term HSCs after irradiation and an overall reduced repopulation capacity[25], and would not be practical in studying the host microenvironment or clonal competition between pathological clones with the host HSCs.

Interestingly, in vivo imaging of the transplanted *Tet2*$^{+/-}$ and WT cells showed that both cell populations tend to localize in the same marrow cavity, whereas individual populations form discrete micro-niches. This observation was found to be consistent across calvaria and long bone metaphysis tissues. These results implied the presence of "favorable" cavities as a shared microenvironment to promote clonal competition. In agreement with this, we have previously shown that bone marrow cavities that activated HSCs and acute myeloid leukemia cells almost exclusively expanded in marrow cavities undergoing active bone remodeling[17,20]. Whether bone remodeling serves as a universal feature to facilitate competition of *Tet2*$^{+/-}$ and WT cells, and the differential downstream mechanisms from the micro-niches remained to be studied. Notably, a substantial population of *Tet2*$^{+/-}$ cells migrated across the bone marrow and showed no stable association with the marrow microenvironment. This phenomenon has been reported in T-cell acute leukemia[49], with an implication that therapeutic targeting towards cell migration and the consequence of niche deterioration during disease propagation. In vivo tracking from the *Tet2*$^{+/-}$ model; however, also revealed the presence of stationary cell compartments and their niche would not be easily captured without imaging guidance.

Despite the preserved marrow microenvironment, a main limitation of using such low-dose irradiation is the higher uncertainty in engraftment. Our studies were performed in the context of syngeneic transplantation; thus, cell engraftment will likely be reduced in allogeneic transplantation. The fact that chimerism was significantly improved when using 1 Gy irradiation (Fig. S1b) suggested the feasibility of optimizing the engraftment using an irradiation dose way below the commonly used sublethal irradiation regimens (4–6 Gy), and the protocols provided in this work will allow the research community to titrate the minimal irradiation dose required to achieve targeted donor chimerism. On a different note, although the local irradiation regimen on the unilateral side of calvaria produced less robust engraftment, it did allow borderline engraftment up to 12–16 weeks post transplantation. It is therefore promising to further characterize the dependency on the size irradiation field, dose, and the irradiation location (e.g. calvaria vs. long bones) to enable satisfactory engraftment while preserving the calvarial bone marrow for intravital imaging. A well studied alternative to low-dose irradiation is the use of KIT mutant (*Kit*$^{W/Wv}$*, or later* the *Rag2*$^{-/-}$ $\gamma_c^{-/-}$ *Kit* $^{W/Wv}$) to enable stable donor cell engraftment. However, it worked on the basis of impaired host cell response to stem cell factor (SCF), depletion of certain immune subsets, and a compensated over-production of SCF from the microenvironment. This may be less representative of the native microenvironment and would not allow investigations of clonal competition between the CHIP clones and the host cells. In comparison, major immune subsets were preserved in 0.5 Gy irradiated mice (Fig. S2a). Despite an upregulated inflammatory responses (Fig. S2b), the transcriptional change did not lead to significant vessel dilation, leakage, or changes in the ability of stromal cells to support LSKs.

One variable that will require further characterizations is that the stress response to irradiation is likely different between young and aged animals and between sexes. Hematopoietic aging is associated with expansion of phenotypic HSCs with increased myeloid bias. Interestingly, this has been linked to faster myeloid recovery in the aged group under sublethal irradiation at 6.5 Gy, yet the neutrophils were found to be defective in chemotaxis. Of note is the greater radio-resistance in aged males than females, likely attributed to an increase in myeloid production in the aged males (faster recovery), and transcriptionally an upregulated interferon response in females that may exhausts HSCs[50]. These studies were in general performed at much higher irradiation doses (6.5–11 Gy) to study hematopoietic acute radiation syndromes. Though fewer differences are expected in the low-dose irradiation regimen, the studies still provided possible rationales when differential *Tet2* engraftment (e.g. higher host defense in aged males) or inflammatory signatures were observed in the aged group. Adult mice and both sexes were used in this study; however, careful data interpretation will be needed to consider the intrinsic age/sex differences in response to irradiation.

In addition, while the study has a major focus on the vascular integrity and MSC functions given their roles in supporting clonal hematopoiesis and MDS, further studies are required to better understand other niche compartments and their potential roles in regulating transplanted cells and the native HSCs. For example, low-level irradiation of 0.5 and 1 Gy has been indicated to potentially promote proliferation and differentiation of osteoblasts[51], which may affect bone homeostasis and regulate the size of HSC pool[52].

To conclude, we leveraged high-resolution live-animal microscopy and with 0.5 Gy whole body or local irradiation to capture single cells and early expansion of benign/pre-malignant clones in the functionally preserved microenvironment. Our results indicated minimal inflammation after the radiation insult and preservation of the stromal niche. Using live animal imaging, this strategy showed for the first time that *Tet2*$^{+/-}$ and WT cells may utilize a shared microenvironment, but distinct micro-niches in the marrow at the disease initiating stage. Future work will be focused on in vivo tracking of cell-niche interactions and spatially resolved molecular analyses to decode the niche profiles in these hot spots, which are otherwise not resolvable via bulk analyses. The technique

developed in this work may be further optimized to minimize the irradiation surface area and can be broadly applied to study other bone marrow failure disorders.

Materials and methods

Animals

All animal experiments conducted in this paper are in accordance and approved by the University of Rochester University Committee on Animal Resources (UCAR) under protocol number UCAR-2022-001E. Experiments were performed in accordance with UCAR ethical standards and guidelines listed in the United States Animal Welfare Act, Public Health Service Policy (University of Rochester D16-00188(A3292-01)), and the Public Health Act of New York State. UCAR is accredited by the Association for the Assessment and Accreditation of Laboratory Animal Care (AAALAC). For all experiments, 2 to 5-month-old adult wild-type C57BL/6 J mice were used (The Jackson Laboratory, Stock No. 000664). $Tet2^{+/-}$ mice were crossed with homozygous UBC-GFP transgenic mice (JAX, Stock No. 004353). Age-matching homozygous DsRed.T3 mice were used in the co-transplantation studies (JAX Stock No. 006051). Animals were all housed and cared for in a temperature and humidity-controlled environment according to the guidelines of the vivarium in the University of Rochester on a 12/12-h light–dark cycle provided with food and water ad libitum.

Whole bone marrow transplantation in irradiated mice and peripheral blood analysis

To allow intravital visualization of healthy or *Tet2*$^{+/-}$ cells, donor cells that carried DsRed or UBI-GFP fluorescent reporters were transplanted into recipient (8 to 12-week-old) C57/BL6 mice. Male mice were used in WBI, co-transplanted and non-irradiated groups. Female mice were used in focal, and limb irradiated groups. Mice were whole body irradiated (WBI) using a Cs irradiator operating at a dose of 0.5 Gy with a 2- to 6-h interval before transplantation. For local irradiation, SARRP X-irradiator (Small Animal Radiation Research Platform; XStrahl Inc, Suwanee, Georgia) was used to precisely deposit 0.5 Gy on the right side of the frontal and parietal bone under CT-guidance. To harvest whole bone marrow cells, two million whole bone marrow cells harvested from long bones were transplanted via retro-orbital injection through the right eye into anaesthetized mice. Peripheral blood analysis of transplanted recipients was performed to confirm the percentage of donor engraftment. Approximately 2–3 drops of tail blood were collected at 4-week intervals and analyzed for up to 30 weeks after transplantation. Peripheral blood was treated with 300 µl of 5 mM EDTA (Invitrogen, AM9260G), followed by addition of 2% Dextran (Spectrum Chemical, 18-602-090) and placed in a 37 °C metallic beads for an hour. Cell suspension in 5% FACs (Gemini Bio, 900-208) buffer were treated with red blood cell lysis buffer for 5 min (Invitrogen, 00-4333-57). The samples were then stained with dead cell stains, propidium iodide (Invitrogen, P3566) or DAPI (Invitrogen, D21490), before analyses. The percentage of engraftment was analyzed using GFP^+ cells out of the total live cells. All data were collected using a BD LSRFortessa (FACSDIVA software) and were processed using FlowJo (v10.9/10.10).

Intravital imaging

Mice were anesthetized using an induction dose of 3% isoflurane followed by a maintenance dose of 1.25–1.5%. The toe pinch method and respiratory frequency were used to confirm a suitable level of anesthesia in the mice. To minimize pain, mice also received Buprenorphine SR at a dosage of 0.5–1.0 mg/kg. The hair on the calvarium was shaved and the skull was exposed by creating a skin flap. The calvarial bone was then mounted using a heated mouse restrainer and intravital imaging was performed as previously described[17], using a polygon-scanning video-rate two-photon microscope (Bliq Photonics, Québec, Canada). In brief, a femtosecond laser beam generated from a Mai-Tai laser was focused onto the sample through a 25X, NA1.1 water-immersion objective (Nikon N25X-APO-MP) that yields a field of view of 333 × 333 µm. The laser power of ~ 60 mW was used to image the bone marrow. Two-photon excitation at 920 nm were used to simultaneously excite GFP, DsRed, and the vascular contrast. Excitation at 810 nm was used to visualize Hoechst 33342. The second harmonic generation (SHG) from the bone and fluorescence emission were collected using the following band pass filters: 439/150 nm or 442/40 nm for SHG and Hoechst 33342, 520/40 nm for GFP or fluorescein-dextran, 630/92 nm for red fluorophores (Rhodamine dextran, propidium iodide). Volumetric stacks were acquired with a 3- or 5- µm step size from the calvaria surface. Based on the frame rate of 30 frames per second, 10–30 frames were averaged to acquire a single image. For in vivo live/dead imaging, WT mice were imaged on Day1 after 0.5 Gy WBI. A mixture of 70 µL Hoechst 33342 (10 mg/mL, H3570), 60 µL propidium Iodide (1 mg/mL, P3566) and 70 µL dextran-conjugated fluorescein (70 kDa, 12.5 mg/mL in PBS, D1823) were administered via retro-orbital injection to label live cells, dead cells, and vasculature, respectively. Imaging was performed at 15 min after injection to allow sufficient cell labeling.

Image analyses

Vessel permeability was measured based on quantitative analysis described previously[37]. In brief, Rhodamine B conjugated dextran (70,000 MW) was administered through retro-orbital injection while performing video-rate image acquisition (15–30 frames per second) at a fixed field of view for 2 min. As the solute diffuses out of the vessel, the permeability was calculated by looking at intensity values from region of interest closest to the vessel. The relationship between permeability, ROI volume, and change in dye intensity can be described by the following equation:

$$P = \frac{V}{A} * \frac{dI}{dt} * \frac{1}{I_{in} - I_{out}}. \quad (1)$$

P represents the permeability of the vessel, V is the volume of the selected ROI next to the vessel, and A is the area of the ratio of vessel surface area to the total area of the ROI. Here, the dI/dt is representative of the linear slope within the intensity change trendline within the ROI for the first 5–40 s of capture. Lastly, I_{in} is the intensity of the vessel at the beginning of the measurement, while I_{out} is the intensity of the ROI at the beginning of the measurement.

Vessel density was calculated by vascular voxel size per selected field of views (FOVs). Vessels were segmented using Trainable Weka Segmentation[53] to obtain binarized images and the FOVs were taken from calvarial bone marrow regions of frontal bones.

To quantify cell viability via in vivo imaging, the number of cells stained with propidium iodide were counted manually per segmented volume of a bone marrow cavity[17] (a 3D inclusion of the first 40–60 μm from the endosteum). As osteocytes and the lacuna space tend to accumulate fluorescent probes, the signals from osteocytes were excluded throughout the calculation.

The locations of $Tet2^{GFP}$ and WT^{DsRed} cells were annotated manually for each segmented bone marrow cavity. The distance from each cell to every other cell was calculated to obtain the minimum inter-cellular distance within the same population or between populations. Individual bone marrow cavities were characterized as $Tet2^{GFP}$ only, WT^{DsRed} only, or both cells present.

Tri-lineage differentiation assays of MSCs

MSCs were harvested from the long bone of 0.5 Gy whole body irradiated mice at one week after irradiation, and from a set of sex/age-matched non-irradiated control group. The MSC isolation procedures are based on the protocols described previously (Manuscript under review)[54]. In brief, bone marrow plugs were flushed with 23G needle into collagen coated (Corning #354236) 10-cm plate containing 10 mL of complete αMEM (Gibco A10490-01), supplemented with 15% FBS (Gemini Bio, 100-500-500) and 1% Penicillin/ Streptomycin (Gibco 15140122). The bone marrow plug was incubated for 5 days in hypoxic (5% oxygen) condition, followed by media change. After 1 day in the fresh media, cells were trypsinized with Tryple Express (Gibco 12605010) and resuspended for MSC sorting. Approximately 2–3 million cells were stained with lineage markers (CD3e, B220, Ter119, Gr-1), CD45, F4/80, CD31, DAPI, Ly6C, Sca-1, and CD51, and the MSCs were sorted based on $DAPI^-$, $CD45^-$, Lin^-, $CD31^-$, $F4/80^-$, Ly6C-, $Sca\text{-}1^+$, and $CD51^+$ gating. The sorted MSCs were seeded in a collagen-coated 6-well plate at a seeding density of 1.5×10^4–3×10^4 cells per well and incubated in complete αMEM under 5% oxygen. After 2–5 passages, 1×10^5 cells were seeded onto 10-mm collagen coated coverslips placed in the 12-well plates for confluency followed by tri-lineage differentiation assays. In brief, cells are cultured with osteogenic differentiation media (100 ml complete αMEM, 50 μg/ml Ascorbic acid, 10 mM Beta-glycerol-phosphate, 100 nM Dexamethasone) or in chondrogenic differentiation media (95 ml Mesencult™-ACF chondrogenic differentiation kit, Stem Cell Technologies), with media change every 3 days for 14 days. For adipogenic differentiation, cells were incubated in the media for 3 days (100 ml complete αMEM, 1 mM Rosiglitazone, 1 μM Dexamethasone, 125 μM IBMX, 50 mU/ml Insulin R), followed by incubation in new media (100 ml complete αMEM, 50 mU/ml Insulin R) for 1 day and alternating for the remainder of the 14 days. Before quantifications, cells were washed with 1 × PBS and fixed with 10% neutral formalin and stained with 2% Alizarin Red (pH 4.2), 0.2% Oil Red O, and 1% Alcian Blue (pH 2.5) for osteogenic, adipogenic, and chondrogenic assays, respectively. Cells on the coverslips were then imaged with bright field and epi-fluorescence microscope. Quantifications was based on the number of stained cells normalized to the total number of cells on a quadrant of the coverslip using FIJI.

MSC co-culture and LSK transplantation assays

The effect of 0.5 Gy WBI on MSC support of HSCs was assessed with irradiated MSCs being cocultured with LSK (Lin^-, $Sca1^+$, $c\text{-}kit^+$) cells. 1×10^5 MSC cells were cultured in collagen-coated 6-well plates for 3 days (αMEM supplemented with 10% FBS, 1% Penicillin/Streptomycin) until 90–95% confluency. 4,000 sorted GFP^+ LSK cells were then added and co-cultured with MSCs for 3 days before competitive transplantation assays (RPMI supplemented with 10% FBS, β-mercaptoethanol, and Penicillin/Streptomycin). Before transplantation, the recipient mice were irradiated with a split dose of 12 Gy with a 3-h interval between the two 6-Gy doses. The co-cultured GFP^+ LSK/MSC cells were transplanted with GFP^- 2×10^6 whole bone marrow cells via retroorbital injection. Chimerism was assessed every 4 weeks over the course of 16 weeks.

Bone marrow interstitial fluid isolation and ELISA assay

CXCL12(SDF-1) levels in the bone marrow interstitial fluid were assessed using an ELISA DuoSet kit (R&D system DY460) and DuoSet ELISA Ancillary Reagent kit (R&D system DY008B). Mice (wild-type littermates) between the ages of 2–5 months were non-conditioned or irradiated at 0.5 Gy and 4.5 Gy WBI. All femur, tibia and pelvis bones (6 bones total) were isolated and crushed in 3 mL sterile PBS (Gibco 20012-027) until translucent. Supernatant was centrifuged at 1200 rpm, 4 °C, for 5 min, and repeated at the same setting. The final supernatant solution was stored at -80 C. CXCL12 ELISA plate preparation and assay were performed under general ELISA protocol provided by R&D systems and run on a BioTex plate reader (BioTex Synergy Mx).

Single cell RNA sequencing (10X genomics)

scRNA sequencing samples were processed using 10 × Genomics platform, prepared by the Genomics Research Core at University of Rochester Medical Center. Single cell suspensions derived from 0.5 Gy irradiated mice calvaria were counted and captured using the Chromium Controller. Libraries were then prepared using Chromium Single Cell 3 v2 Reagent kits and sequenced on the NovaSeq 6000 (Illumina, 100,000 reads per cell). Read count matrices were obtained by aligning the reads to the mm10 mouse reference genome using Cellranger (v3.0.2, 10 × Genomics) and analyzed using Seurat[55]. Differential analyses was performed with published

datasets of non-conditioned calvarial bone marrow[20] (GEO database GSE188902: GSM5691724; GSM5691725; GSM5691727).

Statistics and reproducibility

Data are expressed as mean ± standard deviation. P values were calculated using Mann–Whitney test or unpaired, two-tailed Student's t-test based on normality (GraphPad Prism). P values < 0.05 were considered as significant difference. Sample size 'n' indicates biological replicates, while 'N' indicates the number of animals per group. No animals were excluded from the analysis.

Data availability

All data needed to evaluate the conclusions in the paper are present in the paper and the supplementary materials. Source data will be provided with the paper.

Received: 9 May 2024; Accepted: 27 August 2024
Published online: 03 September 2024

References

1. Jaiswal, S. et al. Clonal hematopoiesis and risk of atherosclerotic cardiovascular disease. *N. Engl. J. Med.* **377**, 111–121 (2017).
2. Bowman, R. L., Busque, L. & Levine, R. L. Clonal hematopoiesis and evolution to hematopoietic malignancies. *Cell Stem Cell* **22**, 157–170 (2018).
3. King, K. Y., Huang, Y., Nakada, D. & Goodell, M. A. Environmental influences on clonal hematopoiesis. *Exp. Hematol.* **83**, 66–73 (2020).
4. Hormaechea-Agulla, D. et al. Chronic infection drives Dnmt3a-loss-of-function clonal hematopoiesis via IFNγ signaling. *Cell Stem Cell* **28**, 1428-1442.e6 (2021).
5. Sanmiguel, J. M. et al. Distinct tumor necrosis factor alpha receptors dictate stem cell fitness versus lineage output in Dnmt3a-mutant clonal hematopoiesis. *Cancer Discov.* **12**, 2763–2773 (2022).
6. Pietras, E. M. et al. Chronic interleukin-1 drives haematopoietic stem cells towards precocious myeloid differentiation at the expense of self-renewal. *Nat. Cell Biol.* **18**, 607–618 (2016).
7. Mitchell, C. A. et al. Stromal niche inflammation mediated by IL-1 signalling is a targetable driver of haematopoietic ageing. *Nat. Cell Biol.* **25**, 30–41 (2023).
8. Avagyan, S. et al. Resistance to inflammation underlies enhanced fitness in clonal hematopoiesis. *Science* **1979**(374), 768–772 (2021).
9. Caiado, F. et al. Aging drives $Tet2^{+/-}$ clonal hematopoiesis via IL-1 signaling. *Blood* **141**, 886–903 (2023).
10. Meisel, M. et al. Microbial signals drive pre-leukaemic myeloproliferation in a Tet2-deficient host. *Nature* **557**, 580–584 (2018).
11. Zhang, J. et al. In situ mapping identifies distinct vascular niches for myelopoiesis. *Nature* **590**, 457–462 (2021).
12. Acar, M. et al. Deep imaging of bone marrow shows non-dividing stem cells are mainly perisinusoidal. *Nature* **526**, 126–130 (2015).
13. Comazzetto, S. et al. Restricted hematopoietic progenitors and erythropoiesis require SCF from Leptin receptor+ Niche cells in the bone marrow. *Cell Stem Cell* **24**, 477-486.e6 (2019).
14. Shen, B. et al. A mechanosensitive peri-arteriolar niche for osteogenesis and lymphopoiesis. *Nature* **591**, 438–444 (2021).
15. Pinho, S. et al. Lineage-biased hematopoietic stem cells are regulated by distinct niches. *Dev. Cell* **44**, 634-641.e4 (2018).
16. Sipkins, D. A. et al. In vivo imaging of specialized bone marrow endothelial microdomains for tumour engraftment. *Nature* **435**, 969–973 (2005).
17. Christodoulou, C. et al. Live-animal imaging of native haematopoietic stem and progenitor cells. *Nature* **578**, 278–283 (2020).
18. Bruns, I. et al. Megakaryocytes regulate hematopoietic stem cell quiescence through CXCL4 secretion. *Nat. Med.* **20**, 1315–1320 (2014).
19. Grockowiak, E. et al. Different niches for stem cells carrying the same oncogenic driver affect pathogenesis and therapy response in myeloproliferative neoplasms. *Nat. Cancer* **4**, 1193–1209 (2023).
20. Haase, C. et al. Image-seq: Spatially resolved single-cell sequencing guided by in situ and in vivo imaging. *Nat. Methods* **19**, 1622–1633 (2022).
21. Oguro, H., Ding, L. & Morrison, S. J. SLAM family markers resolve functionally distinct subpopulations of hematopoietic stem cells and multipotent progenitors. *Cell Stem Cell* **13**, 102–116 (2013).
22. Lo Celso, C. et al. Live-animal tracking of individual haematopoietic stem/progenitor cells in their niche. *Nature* **457**, 92–6 (2009).
23. Park, E. et al. Bone marrow transplantation procedures in mice to study clonal hematopoiesis. *J. Vis. Exp.* https://doi.org/10.3791/61875-v (2021).
24. Wang, Y. et al. Tet2-mediated clonal hematopoiesis in nonconditioned mice accelerates age-associated cardiac dysfunction. *JCI Insight* https://doi.org/10.1172/jci.insight.135204 (2020).
25. Calvi, L. M. et al. Acute and late effects of combined internal and external radiation exposures on the hematopoietic system. *Int. J. Radiat. Biol.* **95**, 1447–1461 (2019).
26. Bouten, R. M. et al. Effects of radiation on endothelial barrier and vascular integrity. In *Tissue Barriers in Disease, Injury and Regeneration* (ed. Bouten, R. M.) 43–94 (Elsevier, 2021). https://doi.org/10.1016/B978-0-12-818561-2.00007-2.
27. Pronk, E. & Raaijmakers, M. H. G. P. The mesenchymal niche in MDS. *J. Am. Soc. Hematol.* **133**, 1031–1038 (2019).
28. Méndez-Ferrer, S. et al. Mesenchymal and haematopoietic stem cells form a unique bone marrow niche. *Nature* **466**, 829–834 (2010).
29. Yue, R., Zhou, B. O., Shimada, I. S., Zhao, Z. & Morrison, S. J. Leptin receptor promotes adipogenesis and reduces osteogenesis by regulating mesenchymal stromal cells in adult bone marrow. *Cell Stem Cell* **18**, 782–796 (2016).
30. Sarhan, D. et al. Mesenchymal stromal cells shape the MDS microenvironment by inducing suppressive monocytes that dampen NK cell function. *JCI Insight* https://doi.org/10.1172/jci.insight.130155 (2020).
31. Agarwal, P. et al. Mesenchymal niche-specific expression of Cxcl12 controls quiescence of treatment-resistant leukemia stem cells. *Cell Stem Cell* **24**, 769-784.e6 (2019).
32. Zambetti, N. A. et al. Mesenchymal inflammation drives genotoxic stress in hematopoietic stem cells and predicts disease evolution in human pre-leukemia. *Cell Stem Cell* **19**, 613–627 (2016).
33. Baccin, C. et al. Combined single-cell and spatial transcriptomics reveal the molecular, cellular and spatial bone marrow niche organization. *Nat. Cell Biol.* **22**, 346 (2020).
34. Azadniv, M. et al. Bone marrow mesenchymal stromal cells from acute myelogenous leukemia patients demonstrate adipogenic differentiation propensity with implications for leukemia cell support. *Leukemia* **34**, 391–403 (2020).
35. Gerosa, R. C. et al. CXCL12-abundant reticular cells are the major source of IL-6 upon LPS stimulation and thereby regulate hematopoiesis. *Blood Adv.* **5**, 5002–5015 (2021).

36. Duarte, D. et al. Inhibition of endosteal vascular niche remodeling rescues hematopoietic stem cell loss in AML. *Cell Stem Cell* **22**, 64-77.e6 (2018).
37. Itkin, T. et al. Distinct bone marrow blood vessels differentially regulate haematopoiesis. *Nature* **532**, 323–328 (2016).
38. McKelvey, K. J., Hudson, A. L., Back, M., Eade, T. & Diakos, C. I. Radiation, inflammation and the immune response in cancer. *Mamm. Genome* **29**, 843–865 (2018).
39. Ali, A. et al. Adaptive preservation of orphan ribosomal proteins in chaperone-dispersed condensates. *Nat. Cell Biol.* **25**, 1691–1703 (2023).
40. Jiao, Y., Cao, F. & Liu, H. Radiation-induced cell death and its mechanisms. *Health Phys.* **123**, 376–386 (2022).
41. Luis, T. C. et al. Perivascular niche cells sense thrombocytopenia and activate hematopoietic stem cells in an IL-1 dependent manner. *Nat. Commun*. https://doi.org/10.1038/s41467-023-41691-y (2023).
42. Kaszuba, C. M. et al. Identifying bone marrow microenvironmental populations in myelodysplastic syndrome and acute myeloid leukemia. *J. Vis. Exp.* https://doi.org/10.3791/66093 (2023).
43. Baselet, B., Sonveaux, P., Baatout, S. & Aerts, A. Pathological effects of ionizing radiation: Endothelial activation and dysfunction. *Cell. Mol. Life Sci.* **76**, 699–728 (2019).
44. Peslak, S. A. et al. EPO-mediated expansion of late-stage erythroid progenitors in the bone marrow initiates recovery from sublethal radiation stress. *Blood* **120**, 2501–2511 (2012).
45. Meacham, C. E. et al. Adiponectin receptors sustain haematopoietic stem cells throughout adulthood by protecting them from inflammation. *Nat. Cell Biol.* **24**, 697–707 (2022).
46. Zhou, B. O. et al. Bone marrow adipocytes promote the regeneration of stem cells and haematopoiesis by secreting SCF. *Nat. Cell Biol.* **19**, 891–903 (2017).
47. Fujishiro, A. et al. Effects of acute exposure to low-dose radiation on the characteristics of human bone marrow mesenchymal stromal/stem cells. *Inflamm. Regen.* https://doi.org/10.1186/s41232-017-0049-2 (2017).
48. Sweeney-Ambros, A. R., Nappi, A. N. & Oest, M. E. In vitro radiosensitivity of murine marrow stromal cells varies across donor strains. *Radiat. Res.* **195**, 590–595 (2021).
49. Hawkins, E. D. et al. T-cell acute leukaemia exhibits dynamic interactions with bone marrow microenvironments. *Nature* **538**, 518–522 (2016).
50. Patterson, A. M. et al. Age and sex divergence in hematopoietic radiosensitivity in aged mouse models of the hematopoietic acute radiation syndrome. *Radiat. Res.* **198**, 221–242 (2022).
51. Chen, M. et al. Low-dose X-ray irradiation promotes osteoblast proliferation, differentiation and fracture healing. *PLoS One* **9**, e104016 (2014).
52. Zhang, H. et al. The roles of bone remodeling in normal hematopoiesis and age-related hematological malignancies. *Bone Res.* https://doi.org/10.1038/s41413-023-00249-w (2023).
53. Arganda-carreras, I. et al. Trainable Weka Segmentation: A machine learning tool for microscopy pixel classification. *Bioinformatics* **33**, 2424–2426 (2017).
54. Kawano, Y. et al. Persistent contamination by bone and bone marrow-derived macrophages obscures functional assessment of tissue-dependent heterogeneity in mesenchymal stromal cells. *Blood* **142**, 5623 (2023).
55. Butler, A., Hoffman, P., Smibert, P., Papalexi, E. & Satija, R. Integrating single-cell transcriptomic data across different conditions, technologies, and species. *Nat. Biotechnol.* **36**, 411–420 (2018).

Acknowledgements

We thank members in the Center for Musculoskeletal Research (CMSR) and Wilmot Cancer Institute for valuable discussions, as well as the support of the CMSR histology core, URMC multiphoton imaging core, and the URMC flow cytometry core.

Author contributions

K.L. and W.D. performed experiments, wrote main manuscript text, and performed data analysis. Equal contribution. M.M. performed permeability experiments, wrote main manuscript text and performed data analysis. C.H. performed imaging experiments of non-conditioned mice and performed data analysis. Z.Y. drafted code and assisted with data analysis. Y.K. gave guidance on in-vitro MSC culture, LSK/MSC co-culture and flow sorting. C.K. gave guidance on LSK isolation and purification. H.K. gave guidance on in-vitro MSC culture and flow sorting. E.Q. gave guidance and assisted with ELISA assay. B.M. assisted and gave guidance with focal irradiation conditioning. M.B. guided the project towards focal irradiation. J.B. provided insight on LSK isolation and purification. L.M.C. provided guidance on project and edited the manuscript. S.C.Y. supervised the project, edited the manuscript, and gave final approval.

Funding

This study was supported by awards from Vera and Joseph Dresner Foundation to S-C A. Yeh, National Institute on Aging, United States, AG079556 and National Cancer Institute, United States, CA266617.

Competing interests

The authors declare no competing interests.

Arrive guidelines

Data reported in the paper are in accordance with ARRIVE 2.0 guidelines and checklist.

Additional information

Supplementary Information The online version contains supplementary material available at https://doi.org/10.1038/s41598-024-71307-4.

Correspondence and requests for materials should be addressed to S.-C.A.Y.

Reprints and permissions information is available at www.nature.com/reprints.

Publisher's note Springer Nature remains neutral with regard to jurisdictional claims in published maps and institutional affiliations.

Open Access This article is licensed under a Creative Commons Attribution-NonCommercial-NoDerivatives 4.0 International License, which permits any non-commercial use, sharing, distribution and reproduction in any medium or format, as long as you give appropriate credit to the original author(s) and the source, provide a link to the Creative Commons licence, and indicate if you modified the licensed material. You do not have permission under this licence to share adapted material derived from this article or parts of it. The images or other third party material in this article are included in the article's Creative Commons licence, unless indicated otherwise in a credit line to the material. If material is not included in the article's Creative Commons licence and your intended use is not permitted by statutory regulation or exceeds the permitted use, you will need to obtain permission directly from the copyright holder. To view a copy of this licence, visit http://creativecommons.org/licenses/by-nc-nd/4.0/.

© The Author(s) 2024